



Akademie věd České republiky
Ústav teorie informace a automatizace

Academy of Sciences of the Czech Republic
Institute of Information Theory and Automation

RESEARCH REPORT

JIŘÍ FILIP

Towards Effective Measurement and Interpolation of Bidirectional Texture Functions

No. 2298

8 April 2011

ÚTIA AV ČR, Pod vodárenskou věží 4, 182 08 Prague, Czech Republic
E-mail: filipj@utia.cas.cz
Tel: +420 266 052 365
Fax: +420 284 683 031

Towards Effective Measurement and Interpolation of Bidirectional Texture Functions

Jiří Filip

Institute of Information Theory and Automation of the AS CR, Czech Republic

Abstract

Bidirectional texture function (BTF) is acquired by taking thousands of material surface images for different illumination and viewing directions. This function, provided it is measured accurately, is typically exploited for visualization of material appearance in visual accuracy demanding applications. However, accurate measurement of the BTF is time and resources demanding task. While the sampling of illumination and viewing directions is in all known measurement systems done uniformly, we believe that to be more effective the sampling should be tailored specifically to reflectance properties of materials to be measured. Hence, we introduce a novel method of sparse BTF sampling. The method starts with collecting information about material visual behavior by means of small initial subset of reflectance samples measurement and analysis. This information is fed into our heuristic algorithm producing sparse material dependent sampling that is consequently used for BTF measurement and interpolation. The algorithm was tested in simulated measurement test with ten BTF samples, their estimated image subsets were selected, the remaining images were interpolated, and results were computationally and psychophysically compared with the measured data. In average the number of sampling points was less than half the number of original measurements points, and for most materials the produced BTF renderings were perceptually indiscernible from the originals.

1 Introduction

Capturing of accurate material surface appearance is required by many quality demanding application as virtual prototyping, safety simulation, or culture heritage digitization. Generally feasible approach for surface appearance acquisition is sampling illumination and view dependent surface appearance in a form of *bidirectional texture function* (BTF) [DvGNK99]. This seven dimensional function $BTF(\lambda, x, y, \theta_i, \varphi_i, \theta_v, \varphi_v)$ describes spectral (λ), spatial (x, y), and directional ($\theta_i, \varphi_i, \theta_v, \varphi_v$) dependence of surface points reflectance. Each surface point can be represented by a dedicated apparent BRDF function (ABRDF). The BTF is in practice measured as a collection of surface images sampled in fixed illumination and viewing directions. Several ways of BTF measurement exist dependent on a way the required four degrees of freedom of illuminating and sensing equipment are realized. They are based either on mechanically adjustable setups (gonioreflectometer, parabolic mirrors) or static setups without any moving elements (kaleidoscope principle, camera arrays). A recent overview of BTF measurements setups is given in [FH09].

All these setups sampled hemisphere of possible illumination/viewing directions over material sample uniformly. Such a sampling is intuitively correct as it captures continuously changes of material reflectance. Uniform sampling is also handy for BTF rendering and interpolation algorithms where each viewing direction contains the same number of hemispherically distributed illumination directions and vice versa. However, considerable drawback of such a sampling occurs when material exhibits atypical reflectance behavior, e.g., sharp specular highlight, complex occlusion effects in material structure. In such cases the uniform sampling might miss important visual information which cannot be re-

trieved by interpolation from closest measured images. Of course this can be, to certain extent, rectified by increased sampling density, however, it is difficult to determine this density prior to the measurement.

Due to nature of the real-world materials meso- and micro-structure, illumination/view dependency vary significantly from material to material. However, in most cases there is significant redundancy in angularly uniformly sampled reflectance. This redundancy is usually tackled by compression approaches (e.g., PCA, spherical harmonics, reflectance models, probabilistic models - [FH09]). The aim of this project is to approach the problem from the other side, i.e., instead of performing lengthy measurement and data compression in post-processing step, we suggest to measure surface reflectance sparsely and interpolate the remaining data from these sparse measurements. Benefits of the latter approach is faster measurement and higher accuracy.

Main contributions and novelties of this research are:

- Fast heuristic method for automatic material-based estimation of proper sparse illumination/view dependent sampling.
- Method of efficient and accurate interpolation of missing samples from the estimated sparse sampling.
- A psychophysically derived and validated approach for material-based sampling density estimation.

The report is further structured as follows. Section 2 discusses previous work in the area, and Section 3 describes test datasets. Section 4 explains the principle of the sparse sampling estimation method and the following interpolation procedure, while Section 5 computationally and psychophysically evaluates the method's performance, and Section 6 proposes and verifies approach of automatic sampling density prediction. Finally Section 7 concludes the paper.

2 Prior Work

Methods of adaptive sampling of reflectance fields were studied extensively in the past [FBLS07], however, their extension from two dimensional space of illumination directions (θ_i, φ_i) to four dimensional space of illumination and viewing directions ($\theta_i, \varphi_i, \theta_v, \varphi_v$) imposes higher demands on robustness and speed of sampling and interpolation algorithms.

There were already approaches for adaptive BRDF measurements of incoming / outgoing directions [LLSS03] based on a planning algorithm iteratively reducing uncertainty in of BRDF model's fitted parameters. This method increased accuracy of 3D objects' reflectance renderings with lower number of sparsely measured images. This approach cannot be easily employed for BTF sampling as the BTF can be pixel-wisely decomposed to apparent BRDFs (ABRDF), which unfortunately do not obey illumination and view direction reciprocity and thus cannot be accurately approximated by BRDF models. Additionally, applied single lobe isotropic Lafor-tune model limiting applicability of this approach for anisotropic materials only.

To our best knowledge, the idea of sparse selective BTF sampling has not got any attention so far. All BTF measurement systems proposed so far, sample illumination and view directions uniformly. Such a fixed sampling systems can suffer with improper sampling of specular highlights or their interpolation. Refer to Fig. 6 (the second row *wood d.*) for example of improper angular sampling producing discontinuities of sharp specular highlights. Although systems with lower relative distance of light and camera to the measured sample can increase effective sampling density due to varying incoming and outgoing directions across material sample [RMS*08], this can be practically exploited only for samples having either very regular or almost homogeneous surface structure.

In this report we build on a work of Filip et al. [FCGH08], where compression efficiency of standard BTF compression methods was considerably improved by keeping less than 20% visually important samples (i.e., images). This image subset can represent all the other measurements without loss of objectively perceived visual quality. However, these material-dependent subset were obtained from analysis of complete BTF measurements and cannot be reliably applied for sampling of different, even though similar, materials.

Motivation in our work was to develop a method that can predict such a sparse sampling BTF subsets based on only very limited information about material reflectance properties. As the adaptive sampling methods of BTF would typically require computationally demanding iterative evaluation of reconstruction error on the fly to infer next sampling step or strategy, we focused on selective sampling which estimates complete sampling pattern of incoming/outgoing directions prior to the measurement stage. In development of our sparse sampling method we took advantage of prior knowledge about general illumination/view dependent reflectance (e.g., typical location of specular highlights, higher contrast between specular and diffuse reflection for high illumination/viewing elevation angles, etc.).

To sum up, instead of measuring all images and drop many of them [FCGH08], we suggest different approach, i.e., measure few images and reconstruct the rest of them.

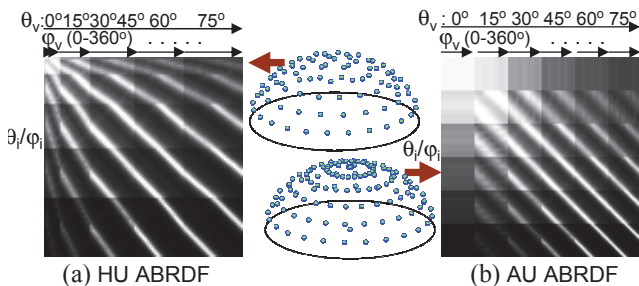


Figure 2: Comparison of (a) hemispherically uniform (HU) and (b) angularly uniform (AU) ABRDF representation. Material *alu*.

3 Test Datasets

Ten material sample measurements from Bonn University BTF database [SSK03]¹ were used for our experiments (aluminum profile, corduroy, dark and light fabrics, dark and light leatherettes, light fabric, dark and light lacquered wood, and knitted wool). Their angular resolution was 81×81 directions distributed uniformly over material hemisphere (shown in Fig. 2-left). Although the sampling density of incoming/outgoing directions in these dataset is relatively low, we believe that these data capture correctly

¹<http://btf.cs.uni-bonn.de/>

major visual features of the original materials. These complete BTF measurements we used as reference data in a simulated measurement experiment, i.e., the datasets were sparsely sampled and interpolated by the proposed algorithm and its performance was verified by comparing with the reference data.

As the proposed sampling was performed in angular domain of incoming/outgoing directions (i.e., individual images as samples), the BTF was decomposed to individual ABRDFs. While the sampling pattern was obtained based on mean ABRDF, the final data interpolation to uniform angular distribution was performed for individual pixels independently. We have considered BRDF representation proposed by Rusinkewitz [Rus98]. While this approach is suitable for BRDF compression by basis functions, discontinuities in ABRDF images produced by this parameterization would require excessively dense sampling. Therefore, we used standard ABRDF representation as image whose rows are incoming directions and columns outgoing directions. The ordering of directions is in a way that elevation angles θ from surface normal are consequently increased and for each such elevation available azimuthal angles φ follow. This corresponds to a spiral-like change of directions from hemisphere top to its bottom. Therefore, the illumination and view directions are distributed uniformly over hemisphere above the measured sample. Example of such a hemispherically uniform (HU) ABRDF representation of the BTF datasets and example of resulting ABRDF image is shown in Fig. 2-left. Although, this provide economical way of BTF measurement the number of samples at individual elevation levels θ_i/θ_v is variable. To avoid variable number of measurements at different elevations, the sparse sampling estimation process is performed in angularly uniform (AU) ABRDF representation (Fig. 2-right).

Contrary to the original HU ABRDF [SSK03], the AU ABRDF over-represents locations near hemisphere pole, however, it allows us representing all combinations of incoming/outgoing elevation angles by the same number of samples (24×24). Each of these regions represents reflectance behavior for variable illumination (rows) and view (columns) azimuthal angles φ_i/φ_v . Such regions are then treated separately during the sparse sampling estimation, while the final sampling is obtained as union of samples from all these regions, and can be transformed back to HU ABRDF.

4 Material-Based Sampling and Interpolation

The principle of the proposed algorithm is outlined in Fig. 1. Individual enumerated parts of the scheme are now discussed more in detail.

① **Initial analysis of material reflectance:** In the first step a small subset of BTF images is measured with motivation to capture most of the information about material reflectance behavior. We selected such illumination/view positions that form couple of slices in angular space (Fig. 1-1). The slice aligned with direction of specular highlights is called *axial slice*, while the slice perpendicular to the highlights is called *diagonal slice*. The diagonal slice captures shape of specular peaks (variable mutual azimuthal position of light and camera), while the axial slice records material anisotropic properties (mutual position of light and camera is fixed and both rotate around sample), i.e. for isotropic samples it is almost straight line. The slices for tested materials at elevation angles $[\theta_i, \theta_v] = [75^\circ, 75^\circ]$ are shown in Fig. 3. For instance samples *alu*, *leath.l.* exhibit strong specularity and isotropy while *fabric l.*, *wood l.*, *wool* show apparent anisotropic reflectance component.

Attenuation and change of distribution of reflectance intensity at different illumination/view elevations are captured by measurement of four of such slices combining θ_i/θ_v at elevations 30° and 75°

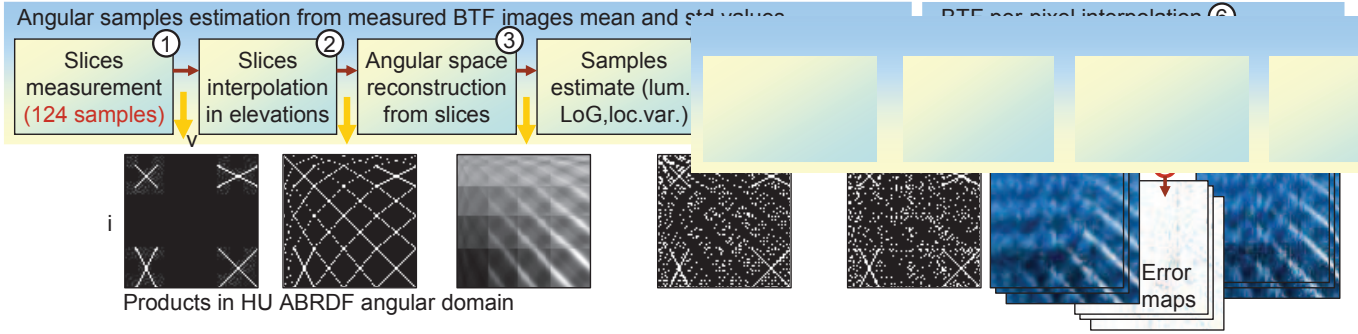


Figure 1: Pipeline of sparse incoming/outgoing directions sampling estimation process, based on mean and standard deviation values computed from initial set of surface reflectance values or images.

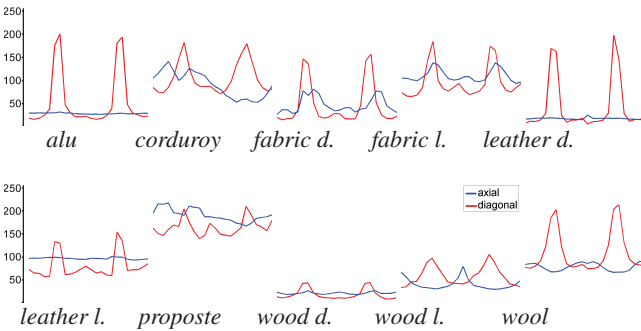


Figure 3: Axial (blue outline) and diagonal (red outline) slices at elevation angles $[\theta_i, \theta_v] = [75^\circ, 75^\circ]$.

(see Fig. 1-1). This is crucial for our sample estimation (explained in point 4), which adapts sampling strategy based on information obtained from the slices. Note that e.g. width of specular peaks differs over the elevations so sampling estimated for high elevation only would not be correct for low elevations, etc. Although in our simulated measurement test the values in the slices represent BTF images, one can in the same way measure single reflectance values only, which might considerably speed up the slices acquisition.

② **Slices interpolation:** The measured slices at four elevation combinations are bilinearly interpolated to account for changes of underlying reflectance profiles at remaining intermediate elevations.

③ **Angular reflectance reconstruction:** Interpolated slices at each combination of incoming/outgoing directions elevations were then used for approximate reconstruction of original reflectance function. This approximative function is obtained by multiplication of the slices for all missing values at a given elevation as shown in Fig. 4. Although this approach do not provide accurate absolute values of real reflectance, it allows capturing of trends of reflectance behavior for a given material sample.

④ **Sparse sampling estimation:** When the estimate of azimuthal-angles-dependent reflectance is reconstructed from the slices, the remaining tasks are selection of such a set of sparse samples and their placement allowing high visual fidelity interpolation of known reconstructed reflectance shape.

The information about slices profiles was used directly for selection of sample candidates. Ridges and valleys of Laplacian of Gaussian

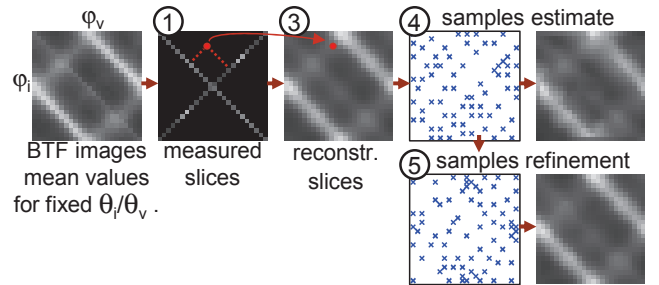


Figure 4: Detailed scheme of samples estimation process at single elevation $[\theta_i/\theta_v] = [75^\circ/75^\circ]$. Material *fabric light*.

(LoG) image filter were suggested [Rob95] as appropriate locations of samples. We tested the LoG filter for selection of sampling candidates, however, much better results were obtained by candidates selection based directly on 1D slices profiles. Here, the LoG filter can be approximated by a second derivation of slice profile (blue outline in Fig. 5-a). In specific shapes of slides' profiles the extrema of second derivation was not sufficient to cover all important sampling points, therefore, we added also extrema points of original slices profile values (red outline in Fig. 5-a). Extrema points of the derivation were taken as axial/diagonal candidates. The sampling candidates were obtained as all combinations of the axial/diagonal candidates (Fig. 5-b). Note, that in the case the slice values are represented by images, and not reflectance values only, the image variance computed in individual slice points can be used as additional, perceptually validated [FCGH08], source of axial/diagonal candidates.

As the number of selected candidates was often very high, and the most of all, the spatial distribution of candidates was close-to-uniform (Fig. 5-b), the candidates were filtered to remove neighboring candidates at positions of slow reflectance changes. To achieve this, the candidates were sequentially tested whether they are far enough apart (threshold $\epsilon_1 = 15^\circ$) from already selected samples and difference of reconstructed reflectance values in compared points is less then defined (threshold $\epsilon_2 = 5$ (from range 0-255)).

During sparse sampling estimation process we have to account for decreasing number of samples towards lower elevation angles θ in HU representation. Hence, we approximate material intensity contrast as difference minimal and maximal values in diagonal slices at measured elevations (red outlines in Fig. 3), interpolate such contrast values across all elevations and use them to modulate thresholds ϵ_1, ϵ_2 . This allows us effectively control number of samples towards lower elevations.

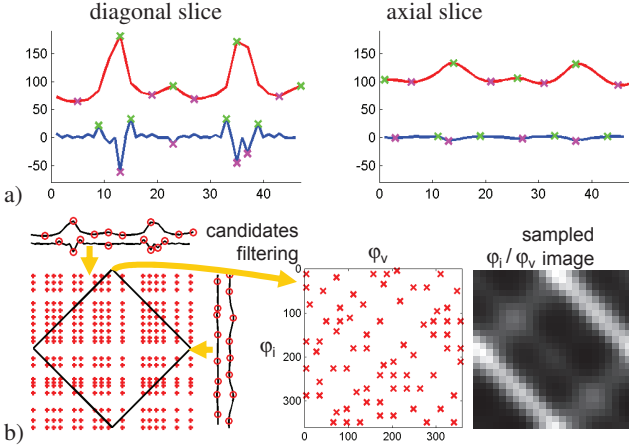


Figure 5: (a) Axial/diagonal candidate points as extrema points of luminance (red) and its second derivation (blue). Local maximal points (green), minimal points (magenta). (b) principle of final sampling points generation from the slides and filtering. Material *fabric light*.

⑤ **Estimated samples refinement:** The sampling of illumination and viewing directions obtained in step 4 works, however, it is still far from optimal performance (see the first row of Fig. 4). However, optimal sample placement problem is NP-complete and thus exhaustive search would take excessively long time. Therefore, we were looking for some computationally effective sub-optimal solution of sample placement. Finally, heuristic algorithm introduced by Robinson and Ren [RR95] was applied for refinement of sample positions obtained in the step 4. The algorithm is based on the idea that a good position to place a sample is where the reconstruction has high error. It starts with initial set obtained in step 4. For each sample the following steps were performed [RR95]:

1. Calculate the reconstruction from other sample points without the current one and rank the reconstruction error on every position of the data array.
2. Choosing the m positions which have the m largest reconstruction errors, place the current sample point in each in turn, recalculating complete interpolation.
3. Rank the m interpolation errors to find the smallest one. If the $\min_m err(m)$ is smaller than the error of interpolation from the original data set, put the current point in that place. Otherwise, leave the point in its previous location.

We have found that $m = 10$ is a good compromise between visual performance and computation time. Generally, this algorithm considerably improved reconstruction performance (see the second row of Fig. 4) at the cost of increase of computation time from ≈ 15 seconds to ≈ 5 minutes.

⑥ **Interpolation from sparse samples:** Selection of interpolation method is crucial for the speed of the proposed sampling algorithm as well as for reconstruction of missing values (non-measured images). The interpolation has to be performed in 4D space of illumination/viewing angles, however, to our knowledge there is not such an efficient interpolation method available so we considered two-steps RBF interpolation [CBC*01], which interpolates values in 3D space. In such a case we would need to interpolate viewing directions first and illumination directions afterwards or vice-versa. Disadvantage of this method is that method's SVD least square fit of data matrix may become ill-conditioned due to either small num-

ber of (or even missing) samples for the particular direction or concentration of the samples (i.e., having similar values), to limited number of directions, e.g., around specular highlight. Although some of these problems might be avoided by data regularization, we decided to exploit well established tools of 2D interpolation. We tested barycentric interpolation, thin-plate splines, and triangle-based linear and cubic interpolations applied directly to interpolation of HU ABRDF images. The best speed-quality trade-off was obtained by the cubic interpolation. This interpolation was used for sampling points estimation (previous step 5) as well as for resampling of whole BTF dataset. As this interpolation do not extrapolate well we added additional 40 mandatory sampling points to the estimated sampling set positioned around image boundary to avoid improperly extrapolated values.

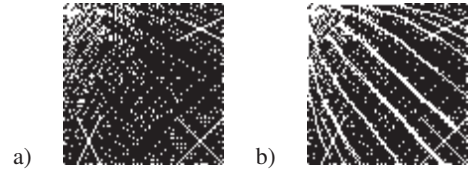


Figure 7: Specular materials: (a) estimated sampling, (b) with additional samples generated along specular lines using linear interpolation from specular samples.

As reproduction of very sharp specular highlights, that some material exhibit (e.g., *wood01*, *wood02*), from a limited number of samples is very difficult, we propose to detect presence of such a sharp highlights from width of peaks in the diagonal slice (red outlines in Fig. 3) and split interpolation in two steps. First, only lines consisting of specular points (corresponding to $|\varphi_i - \varphi_v| = \pi$) are linearly interpolated. Then all interpolated points are added to set of sparse sampling points, while in the second step the data are interpolated by the cubic interpolation from such enlarged sparse sampling set as shown in Fig. 7-b. This guarantees preservation of smooth specular highlights without disruptive holes and minimizing luminance "leaks" out of the highlights, without the increasing a number of measured sampling points. For examples of the proposed ABRDFs interpolation technique refer to Fig. 6, showing final sparse sampling for the tested materials and comparing measured mean ABRDF with its reconstruction from the estimated sampling points. The last row in the figure shows MSE/PSNR/SSIM values computed comparing original and interpolated mean ABRDFs. Please note that the sparse sampling estimation algorithm is independent on a type of interpolation used. Individual spectral planes were interpolated separately.

To save computational costs, the BTFs were seamlessly tiled [SH05] and computation was done on tiles only. The interpolation of one pixel took less than 0.5s so tile of moderate size, e.g., 70×70 pixels took ≈ 40 minutes (Matlab @ Core2Duo 2GHz, 2GB RAM).

5 Tests and Results

Verification of the proposed sparse sampling algorithm performance was done on dataset of rendered images. Two set of such images were generated. The first one contains renderings of original BTF measurements (using 6561 images), while the second one contains renderings based on the proposed sparsely sampled subset of original measurements, where the missing illumination/view combinations were interpolated. Number of samples was selected similar for all material in order to provide reasonable visual quality of interpolated renderings. The renderings represent spherical shape where the BTF is mapped. Although spherical shape was

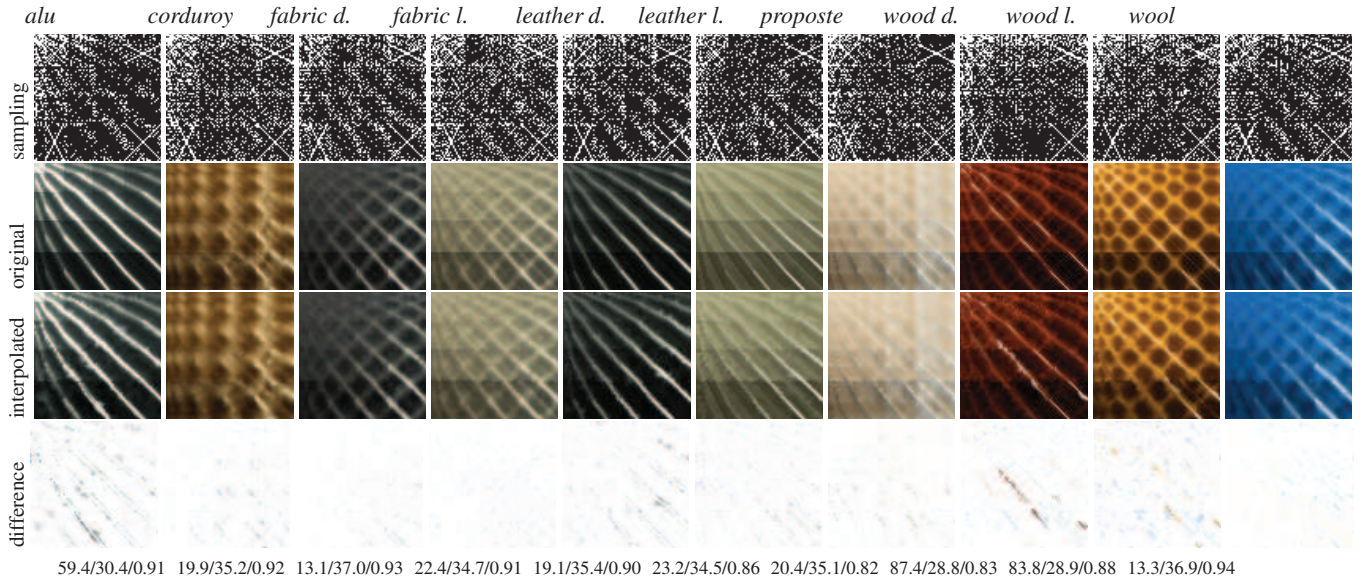


Figure 6: Final sampling patterns obtained by means of our method for ten tested BTF materials (the first row). Number of samples ranged from 1306 to 1702 (original sampling 6561 samples). Measured mean ABRDFs (the second row) compared to those obtained from the selected samples (the third row) and their difference (the fourth row) with MSE/PSNR/SSIM values.

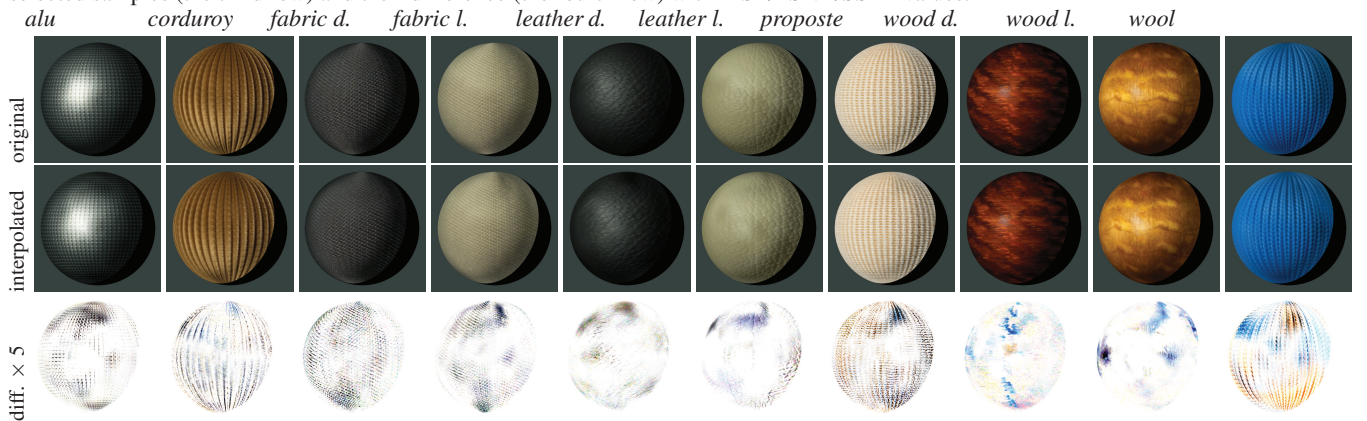


Figure 8: Example rendering using all measurements (6561 samples) (the first row), measurements subset selected and resampled using the proposed method (the second row), difference-map ten-times intensified (the third row).

identified in [VLD07] as inappropriate for testing of visual perception of BRDFs, in [FCGH08] was shown that for structured BTF samples the more complex surface curvature impact subject perception of changes in textured surface appearance. For each tested material were generated four images of sphere rendered for point-light illumination from left, right, top, and bottom respectively, while the viewing direction stayed fixed effectively covering most of the combinations of possible viewing angles. A comparison of rendered target and interpolated images for illumination from left and all tested materials is shown in Fig. 8 side by side with difference maps (five times multiplied).

Resulting couples of rendered images were compared by means of several pixel-wise difference metrics: MSE, PSNR, ΔE in CIE Lab, and SSIM. Results of these metrics for all tested BTF material samples as well as number of samples used for BTF interpolation are shown in Tab. 1.

Although the presented values are encouraging they cannot substitute human judgments. Therefore, we run a psychophysical study on group of ten subjects, showing them couples of rendered images. The study included 160 stimuli showing couples of the orig-

sample	# imgs	MSE	PSNR	CIE ΔE	SSIM
<i>alu</i>	1306	10.23	38.18	1.12	0.951
<i>corduroy</i>	1626	14.70	37.12	1.35	0.949
<i>fabric d.</i>	1521	9.36	38.77	1.32	0.924
<i>fabric l.</i>	1702	7.81	39.48	1.01	0.965
<i>leath.d.</i>	1440	2.91	43.87	0.76	0.971
<i>leath.l.</i>	1368	3.63	43.02	0.77	0.975
<i>proposte</i>	1449	23.28	34.66	1.66	0.927
<i>wood d.</i>	1551	14.89	38.65	1.09	0.976
<i>wood l.</i>	1550	12.30	39.24	1.01	0.984
<i>wool</i>	1473	8.13	39.53	1.40	0.955
AVG	1498	10.72	39.25	1.15	0.958

Table 1: Quality comparison of renderings from original BTF measurements vs. renderings from BTF interpolated using quarter of original samples. Values are average across four images: sphere illuminated from left, right, top, and bottom.

inal renderings as well as couples of original data and interpolated data rendering in a random order. Subjects were asked whether they can see any difference between the images. To avoid lengthy

pixel-wise comparison the viewing time was limited to four seconds, after that the yes/no answer was requested. All subjects had normal or corrected to normal vision and all were naive to a design and purpose of the experiment. Their responses were averaged to obtain response of average human observer. These responses for individual BTF materials are illustrated in Fig. 9-a and show a perceived similarity p_s , i.e., probability that the subjects are not able to distinguish between renderings from original and interpolated data. The materials are numbered in the same order as in Fig. 8. The error bars in the figure represent twice the standard deviation across subjects and four rendered images. The average guess rate (i.e., subjects response to the same images) was 0.075.

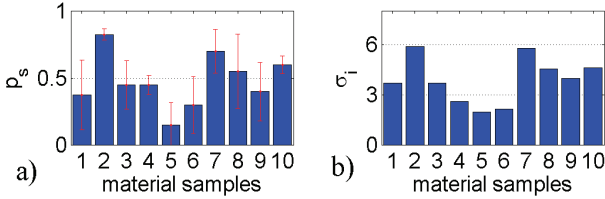


Figure 9: Comparison of (a) perceived similarity from the psychophysical experiment with (b) mean BTF images CIE Luminance variance σ .

6 Sampling Density Prediction

The psychophysical experiment shown different response of human perception to different tested materials even though the number of samples was more or less similar (the second column of Tab. 1). The average probability p_s across the tested materials was 0.48 which represents that only half of the observers was able to distinguish between the images. However, for spatially structured fabrics materials (e.g., *corduroy*, *proposte*, *wool*) the probability was higher than for spatially less variable samples (e.g., *alu*, *leath. d.*, *leath.l.*). As the mean variance of BTF images σ_i was identified as the most perceptually correlated BTF statistics in [FCGH08], we applied similarly the same statistics to BTF CIE luminance values of the tested BTF material samples and obtained values shown in Fig. 9-b. Not surprisingly they are highly correlated with results from the experiment (Pearson correlation coefficient $R = 0.924$). This correlation suggests that materials with lower spatial variance cannot mask the artifacts introduced into data by sparse sampling and following interpolation. Therefore, the number of samples should adapt to material variance. Although the whole BTF measurement is not known before the sparse sampling is realized, we have experimentally verified that variance σ_i can be effectively obtained with similar results from initially measured axial and diagonal slices of BTF images.

Lets assume that user would measure one BTF sample completely for the first time (or take one of the publicly available measurements) and iteratively selects the number of samples k_1 of the proposed sparse sampling algorithm that fulfill its visual fidelity requirements. If the variance of such a sample, computed in slices only, is σ_{i1} , the required number of sparse samples k_N for every new material to be measured with variance σ_{iN} can be roughly predicted as

$$k_N = k_1(\sigma_{i1}/\sigma_{iN}) . \quad (1)$$

This essentially allows automatize not only the estimation of effective material dependent spatial sampling distribution, but also the proper estimation of the number of samples providing the required perceived visual quality.

To validate the proposed material variance-based prediction of number of samples, we selected sample *corduroy* with the current number of samples (1626) as reference sample, as it has the highest perceived similarity in the experiment ($p_s = 0.825$). Then equation 1 was used to predict number of sample images required for the remaining materials. These numbers are shown as k_N in Tab. 2. As the sampling algorithm selects sample candidates as extrema of slices profile and its second derivation, it often happens, most of all for spatially smooth materials, that the number of final samples k is lower than required k_N (bold figures in Tab. 2). Missing samples

	<i>alu</i>	<i>cord.</i>	<i>fabric d.</i>	<i>fabric l.</i>	<i>leath.d.</i>
k_N	2595	1626	2588	3669	4837
k	2347	1626	2435	2653	2529
	<i>leath.l.</i>	<i>propos.</i>	<i>wood d.</i>	<i>wood l.</i>	<i>wool</i>
k_N	4475	1659	2100	2406	2078
k	2608	1700	2180	2403	2064

Table 2: Predicted k_N and applied numbers of samples k . (i.e., BTF images) were then interpolated for all materials and new set of stimuli images were rendered in the same way as for the first experiment. Then a second experiment was performed, in the same way as the previous one, with four subjects from which two of them participated also in the first experiment. Results of perceived simi-

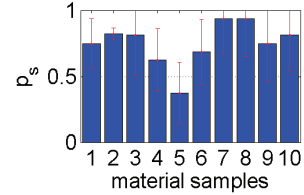


Figure 10: Perceived similarity from the validation experiment.

ilarity, shown in Fig. 10 with average value 0.67, proved our expectation that the differences in stimuli should be less apparent. The average guess rate was 0.05. To achieve even better performance especially for *leather d.* material, one would need more generate more axial/diagonal candidates on slice profiles, preferably by forcing sparse uniformly distributed candidates. Even though, the number of the samples was increased almost twice in average, it is still less than half of original samples while the objectively measured visual performance is almost identical.

7 Conclusions

Our research builds on the fact that each surface material reflectance exhibit unique illumination/view dependent behavior. Hence, we introduce a novel heuristic algorithm for material-dependent illumination/view directions sampling and interpolation of bidirectional texture functions. The sampling is based on analysis of very limited sets of reflectance values, which provides a rough estimation of material illumination and view dependent behavior. Based on this estimate a proper sampling pattern is estimated and refined by sub-optimal search algorithm. Performance of the estimated and interpolated BTF sampling patterns is compared with complete BTF data both computationally and in psychophysical study. The study revealed high correlation of subjects perception with mean variance of BTF images. This variance was further exploited for material dependent estimate sparse sampling density. In average between one quarter and half of the original samples was enough to approach visually indiscernible quality of BTF renderings. Even though, it has to be validated in real measurement experiment, we believe that material dependent sampling of surface appearance allows achieving with the same number of samples a higher accuracy than standard uniform sampling approaches.

As a future work we would like to investigate combination of the proposed method with computationally feasible adaptive sampling.

Acknowledgments

We would like to thank BTF database Bonn for providing their data and the volunteers in the psychophysical study. This work has been supported by the grants GAČR 103/11/0335 and 102/08/0593, EC Marie Curie ERG 239294, and CESNET grants 306 and 387.

References

- CARR J., BEATSON R., CHERRIE J., MITCHELL T., FRIGHT W., MCCALLUM B., EVANS T.: Reconstruction and representation of 3d objects with radial basis functions. *ACM SIGGRAPH 2001, ACM Press* (2001), 67–76.
- DANA K., VAN GINNEKEN B., NAYAR S., KOENDERINK J.: Reflectance and texture of real-world surfaces. *ACM Transactions on Graphics 18*, 1 (1999), 1–34.
- FUCHS M., BLANZ V., LENSCH H. P., SEIDEL H.-P.: Adaptive sampling of reflectance fields. *ACM Trans. Graph.* 26 (June 2007).
- FILIP J., CHANTLER M., GREEN P., HAINDL M.: A psychophysically validated metric for bidirectional texture data reduction. *ACM Transactions on Graphics (Proceedings of SIGGRAPH Asia 2008)* 27, 5 (December 2008), 138.
- FILIP J., HAINDL M.: Bidirectional texture function modeling: A state of the art survey. *IEEE Transactions on Pattern Analysis and Machine Intelligence 31*, 11 (October 2009), 1921–1940.
- LENSCH H. P., LANG J., SÁ A. M., SEIDEL H.-P.: Planned sampling of spatially varying BRDFs. *Computer Graphics Forum* 22, 3 (2003), 473–482.
- RUMP M., MLLER G., SARLETTE R., KOCH D., KLEIN R.: Photo-realistic rendering of metallic car paint from image-based measurements. *Computer Graphics Forum* 27, 2 (2008), 527–536.
- ROBINSON J.: Image coding with ridge and valley primitives. *Communications, IEEE Transactions on* 43, 6 (1995), 2095–2102.
- ROBINSON J. A., REN M. S.: Data-dependent sampling of two-dimensional signals. *Multidimensional Systems and Signal Processing* 6 (1995), 89–111.
- RUSINKIEWICZ S.: A new change of variables for efficient BRDF representation. In *Rendering techniques' 98: proceedings of the Eurographics Workshop in Vienna, Austria, June 29-July 1, 1998* (1998), Springer Verlag Wien, p. 11.
- SOMOL P., HAINDL M.: Novel path search algorithm for image stitching and advanced texture tiling. In *Proceedings of 13-th International Conference in Central Europe on Computer Graphics, Visualization and Computer Vision, WSCG05* (February 2005).
- SATTLER M., SARLETTE R., KLEIN R.: Efficient and realistic visualization of cloth. In *Eurographics Symposium on Rendering 2003* (June 2003).
- VANGORP P., LAURIJSSSEN J., DUTRE P.: The influence of shape on the perception of material reflectance.